Cell PRESS
Immunity
Article

Foxp3$^+$ T Cells Induce Perforin-Dependent Dendritic Cell Death in Tumor-Draining Lymph Nodes

Alexandre Boissonnas,[1,6] Alix Scholer-Dahirel,[1,6] Virginie Simon-Blancal,[1] Luigia Pace,[1] Fabien Valet,[2] Adrien Kissenpfennig,[3] Tim Sparwasser,[4] Bernard Malissen,[3] Luc Fetler,[5,*] and Sebastian Amigorena[1,*]
[1]Institut National de la Santé et de la Recherche Médicale U932, Immunité et Cancer, Institut Curie, F-75245 Paris Cedex 05, France
[2]Institut National de la Santé et de la Recherche Médicale U900, Biostatistics, Institut Curie, F-75245 Paris Cedex 05, France
[3]Centre d'Immunologie de Marseille-Luminy, INSERM, U631, CNRS, UMR6102, Université de la Méditerrannée, Case 906, 13288 Marseille Cedex 9, France
[4]Institute of Infection Immunology, TWINCORE, Centre for Experimental and Clinical Infection Research—a joint venture between the Hannover Medical School (MHH) and the Helmholtz Centre for Infection Research (HZI), Feodor-Lynen-Str. 7, 30625 Hannover, Germany
[5]Centre National de la Recherche Scientifique UMR 168, Laboratoire de Physico-Chimie Curie, Institut Curie, F-75245 Paris Cedex 05, France
[6]These authors contributed equally to this work
*Correspondence: luc.fetler@curie.fr (L.F.), sebastian.amigorena@curie.fr (S.A.)
DOI 10.1016/j.immuni.2009.11.015

SUMMARY

Regulatory T (Treg) cells limit the onset of effective antitumor immunity, through yet-ill-defined mechanisms. We showed the rejection of established ovalbumin (OVA)-expressing MCA101 tumors required both the adoptive transfer of OVA-specific CD8$^+$ T cell receptor transgenic T cells (OTI) and the neutralization of Foxp3$^+$ T cells. In tumor-draining lymph nodes, Foxp3$^+$ T cell neutralization induced a marked arrest in the migration of OTI T cells, increased numbers of dendritic cells (DCs), and enhanced OTI T cell priming. Using an in vitro cytotoxic assay and two-photon live microscopy after adoptive transfer of DCs, we demonstrated that Foxp3$^+$ T cells induced the death of DCs in tumor-draining lymph nodes, but not in the absence of tumor. DC death correlated with Foxp3$^+$ T cell-DC contacts, and it was tumor-antigen and perforin dependent. We conclude that Foxp3$^+$ T cell-dependent DC death in tumor-draining lymph nodes limits the onset of CD8$^+$ T cell responses.

INTRODUCTION

Regulatory T (Treg) cells represent a population of Foxp3-expressing, CD4$^+$, CD25$^+$ T cells that play a key role in the control of autoimmune disorders but also restrict antitumor immune responses (North and Bursuker, 1984). Treg cells represent 5 to 10% of the CD4$^+$ T cells in secondary lymphoid organs and can expand and accumulate in many types of tumors, suggesting that they participate in the inhibition of antitumor immune responses (Wang and Wang, 2007). However, the reasons for Treg cell expansion and accumulation during tumor development, and in particular the antigen specificity of the expanded cells, remain unclear (Hsieh et al., 2004; Pacholczyk et al., 2007). Treg cell accumulation in tumor-bearing animals may result from either proliferation of thymic differentiated Foxp3$^+$ T cells (natural Treg cells) or the conversion of Foxp3$^-$CD4$^+$ T cells into Foxp3$^+$CD4$^+$ T cells (induced Treg cells), depending on the tumor models (Colombo and Piconese, 2007). Because tumor cells might express tumor-associated antigens or tumor-specific antigens, as well as a vast variety of self-antigens, tumor-specific and self-specific Foxp3$^+$ T cells might be present in the tumor microenvironment. These Treg cells may suppress antitumor responses after activation by either tumor-related or tumor-unrelated other self-antigens.

The mechanisms of suppression of antitumor CD8$^+$ T cell responses by Treg cells are still unclear. In certain models, Treg cells suppress priming (Somasundaram et al., 2002; Woo et al., 2002), acting on antigen-presenting cells (Cederbom et al., 2000; Lewkowich et al., 2005; Misra et al., 2004). In other models, Treg cells suppress the effector phase (Appay et al., 2006; Yu et al., 2005) through direct action on T cells, involving IL10 or TGF-β (Ostroukhova et al., 2006; Chen et al., 2005; Green et al., 2003), as well as through IL-2-deprivation (Pandiyan et al., 2007) or cyclic-AMP transfer through gap junctions (Bopp et al., 2007).

A cytotoxic-dependent mechanism for Treg cell suppression has been proposed in several studies. Foxp3$^+$ T cells are cytotoxic to different cell types, including CD8$^+$ T, NK, and B cells, depending on the models, through granzyme B-, perforin-, or Fas-FasL-dependent cytotoxic pathways (Cao et al., 2007; Grossman et al., 2004; Janssens et al., 2003; Zhao et al., 2006). Cao et al. (2007) also show that Treg cells induced in tumor-bearing animals express both perforin and granzyme B. At least in one of these models, target recognition was antigen specific (Janssens et al., 2003), thus selectively targeting MHC class II-expressing antigen-presenting cells.

No doubt that dynamic intravital imaging of Treg cell functions could clarify their mechanisms of action in vivo. Two independent studies in models of diabetes and experimental autoimmune encephalitis have recently imaged Foxp3$^+$ T cells with two-photon intravital microscopy. Both studies concluded that Foxp3$^+$ T cells affect autoreactive naive conventional CD4$^+$ T cell dynamics in lymph nodes (Tadokoro et al., 2006; Tang et al., 2006), thereby preventing their arrest on antigen-presenting cells during priming. These imaging results indicate that Foxp3$^+$ T cell-mediated inhibition of autoimmune responses occurs, at least in part, early during the priming phase in lymph

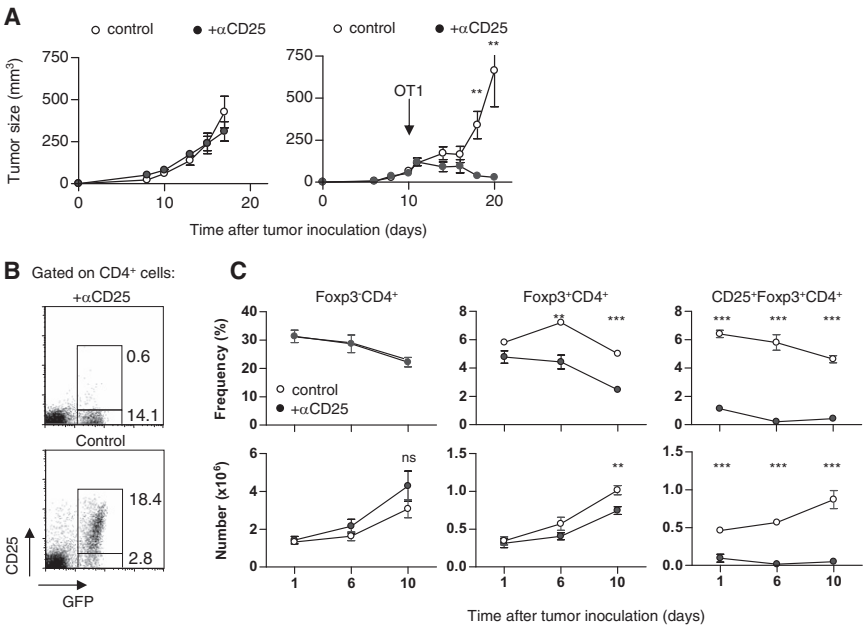

Figure 1. Foxp3+ CD25+ T Cell Neutralization Induces Tumor Rejection after Antigen-Specific CD8+ T Cell Adoptive Transfer

(A) MCA-OVA tumor cells were inoculated in the flank of mice treated (black) or not treated (white) with anti-CD25 (PC61). Naive OTI T cells were adoptively transferred (right panel) or not transferred (left panel) at day 10, and tumor growth was monitored. Graphs represent mean ± SEM values obtained with 22 mice in each group, from five independent experiments (right panel) and eight mice in each group from two independent experiments (left panel).

(B) Representative dot plots of CD25 and GFP expression on CD4+ T cells at d10 in tdLN of Foxp3-EGFP tumor-bearing mice treated or not treated with anti-CD25 as indicated.

(C) The percentage of total cells (upper panels) and absolute numbers (lower panels) of Foxp3−CD4+, Foxp3+CD4+, and CD25+Foxp3+CD4+ cells were monitored 1, 6, and 10 days after treatment with PC61 (black) or rat IgG1 isotype (white). Results are the mean ± SEM of 10 to 13 mice from three to four independent experiments.

nodes. Nevertheless, Foxp3+ T cells also reduce granule exocytosis in effector cytotoxic T lymphocytes (CTLs) in vivo (Mempel et al., 2006). This inhibitory effect did not require long-lasting contacts between Foxp3+ T cells and CTLs, but was dependent on their responsiveness to TGF-β. Altogether, these results show that both the initiation of immune responses in lymph nodes, and the effector phases, may potentially be affected by Foxp3+ T cells. All the imaging experiments in these studies were performed with adoptively transferred, TCR-transgenic, high-affinity Treg cells. Because the affinity of the TCRs influences the dynamics of T cell-DC interactions (Skokos et al., 2007), the analysis of polyclonal Foxp3+ T cells should be very informative.

Here, we have analyzed the interactions between endogenous polyclonal Foxp3+ T cells and DCs in tumor-draining lymph nodes. We have shown that Foxp3+ T cells limit DC survival in the tumor-draining lymph node (tdLN) through an antigen- and perforin-dependent mechanism, involving direct contacts between Foxp3+ T cells and tumor-antigen presenting DCs.

RESULTS

Foxp3+CD25+ T Cells Inhibit Antitumor CD8+ T Cell Responses and Tumor Rejection

To analyze the mechanisms of the Foxp3+ T cell-mediated suppression of antitumor CD8+ T cell responses, we used a methyl-cholanthrene-induced fibrosarcoma cell line, MCA101 (called MCA thereafter), expressing a model antigen, ovalbumin (OVA). MCA-OVA cells grow as solid subcutaneous (s.c.) syngeneic tumors after inoculation in C57Bl/6 (B6) mice (Figure 1A). Injection of anti-OVA transgenic CD8+ T cells (OTI T cells) 10 days after tumor inoculation induced a transient reduction in the rate of tumor growth, but no tumor rejection (Figure 1A). The potential role of Foxp3+ T cells was first addressed with PC61, a CD25 monoclonal antibody previously shown to abolish Treg cell-mediated suppression of antitumor immune responses (Onizuka et al., 1999). The adoptive transfer of OTI T cells to mice previously treated with anti-CD25 induced effective rejection of MCA-OVA (Figure 1A), but not of MCA tumors (not shown).

In order to avoid as much as possible any interference of the anti-CD25 with OTI T cell priming, we injected the anti-CD25 10 days before the adoptive transfer of OTI T cells. At the time of OTI T cell adoptive transfer, the anti-CD25 serum concentration was very low (~100 ng/ml). This serum concentration was 1/10 of the concentration of an isotype control (HRNP, injected under the same conditions), suggesting that the anti-CD25 disappears from the blood (as soon as 2 hr after injection) because of binding to CD25+ cells (Figure S1A available online). In the absence of OTI T cell transfer, anti-CD25 treatment failed to induce tumor rejection (Figure 1A), indicating that the endogenous antitumor immune response was insufficient to reject the tumor in this system.

To investigate the effect of the anti-CD25 treatment on Foxp3+CD25+ T cells, we analyzed their frequency and absolute numbers in the tdLNs, as compared to Foxp3− T cells (Figures 1B and 1C and Figure S1B). The numbers of both CD4+Foxp3+ and CD4+Foxp3− T cells increased after tumor inoculation. The increased number of Foxp3+ T cells in tumor-bearing mice was due to the expansion of natural Foxp3+ T cells, rather than the conversion of CD4+Foxp3− cells to CD4+Foxp3+ cells. Indeed, upon adoptive transfer of CD4+Foxp3− T cells sorted from Foxp3-EGFP mice into tumor-bearing B6 mice, the cells expanded but did not convert to CD4+Foxp3+ T cells (not shown). The most striking effect of the anti-CD25 was a strong reduction of both the absolute numbers and the proportion of CD4+CD25+ T cells. The down modulation of surface CD25 was confirmed with the 7D4 clone, an anti-CD25 recognizing a different epitope from the one used for the injection (not shown). The anti-CD25 did not affect the expansion of CD4+Foxp3−, but reduced by 20%–40% (depending on the experiments) the percentage of Foxp3+ T cells in tdLNs 6–10 days after tumor inoculation (Figure 1C). The anti-CD25 treatment did not deplete Foxp3+ T cells, but affected their accumulation (reduction of 25%, Figure 1C). KI67

staining of Foxp3$^+$ T cells showed that their proliferation was not reduced (not shown). This discrepancy could be explained either by a defect in survival of Foxp3$^+$CD25$^+$ T cells after treatment and/or preferential proliferation of CD4$^+$Foxp3$^+$CD25$^-$ T cells that were not affected by anti-CD25 treatment (Couper et al., 2007; Kohm et al., 2006; Zelenay and Demengeot, 2006). Therefore, even though anti-CD25-treated mice still bear Foxp3$^+$CD25$^-$ T cells, these cells do not suppress tumor rejection by OTI T cells because of their reduced numbers, their decreased activity (due to the lack of CD25 expression), or both.

Tumor inoculation induced a wide activation of Foxp3$^+$ T cells, as reflected by the increased proportion of CD69$^+$ and CD44^{hi} Foxp3$^+$ T cells after tumor inoculation in both tdLNs and non-draining LNs (more than 90% of the Foxp3$^+$ T cells were CD44^{hi} in tumor-bearing mice) showing a systemic activation of Foxp3$^+$ T cells (Figure S1C). Whether these Foxp3$^+$ T cells were specific for self-antigens or tumor-specific antigens is unknown. The percentage of CD62L^{hi} Foxp3$^+$ T cells in the tdLNs increased during tumor growth, suggesting that the CD62L^{lo} Foxp3$^+$ T cells migrated elsewhere. Indeed, we observed that within the tumor, the Foxp3$^+$ T cells exhibited a strongly activated phenotype with high expression of CD44, low expression of CD62L, and a high percentage of CD69^{hi} cells, arguing for a recruitment of antigen-specific Foxp3$^+$ T cells to the tumors. Injection of the anti-CD25 did not modify the proportion of CD69^{hi}, CD44^{hi+}, or CD62L^{hi} Foxp3$^+$ T cells, neither in LNs nor in the tumors (Figure S1C). Therefore, MCA-OVA tumors induce Foxp3$^+$ T cell expansion and activation.

Analysis of Foxp3$^+$ T Cells Motility in Tumor-Draining Lymph Nodes

In order to image endogenous Foxp3$^+$ T cells in lymph nodes, we used B6 knock-in mice expressing an *IRES-EGFP* cassette in the 3′ untranslated region of the *Foxp3* gene (Foxp3-EGFP mice) (Wang et al., 2008). Endogenous Foxp3$^+$ T cells in LNs are organized as a very dense swarm of motile cells that migrate with a mean velocity of 5.8±3.6μm/min (Figures S1D–S1F; Movies S1 and S2). Foxp3$^+$ T cell motility, in terms of mean velocity, confinement ratio, and arrest coefficient, was similar in the LNs of mice bearing tumors or not. In addition, the anti-CD25 treatment did not affect the motility of the remaining Foxp3$^+$ T cells (Figures S1E and S1F). The detailed analysis of the distribution of the motility of the Foxp3$^+$ T cells, revealed the presence of both highly motile (crawling) and nearly arrested cells (swarming) (Figures S1D–S1F). This heterogeneity maybe due to the fact that we imaged polyclonal endogenous Foxp3$^+$ T cells displaying a highly diverse, most likely anti-self antigen-specific, TCR repertoire (Hsieh et al., 2004) (the potential recognition of self epitopes may reduce the global motility of the cells).

The mean velocity observed for polyclonal Foxp3$^+$ T cells is lower than that previously determined for conventional CD4$^+$ T cells (Vmean: ~10 μm/min [Miller et al., 2004]). We therefore compared the motility of endogenous Foxp3$^+$ T cells to that of adoptively transferred CMTMR-labeled naive Marilyn CD4$^+$ T cells, in both tumor-bearing and tumor-free mice (Figure S1E). Interestingly, the motility of Marilyn CD4$^+$ T cells was lower in tdLNs (Vmean: 5.9 ± 2.9 μm/min) than in the same LNs in the absence of tumor (Vmean: 7.8 ± 2.3 μm/min). In contrast, as described above, the mean velocity for Foxp3$^+$ T cells was similarly low in the absence or presence of tumors. This observation suggests that the motility of polyclonal Foxp3$^+$ T cells is lower than conventional CD4$^+$ Foxp3$^-$ T cell motility, in tumor-free animals, but similar in tdLNs. Nevertheless, we cannot exclude that such dissimilarity in the mobility of CD4$^+$Foxp3$^-$ and CD4$^+$ Foxp3$^+$ T cells is due to differences between endogenous and adoptively transferred T cells.

Foxp3$^+$CD25$^+$ T Cells Inhibit the Arrest of Antitumor CD8$^+$ T Cells in Tumor-Draining Lymph Nodes

We have shown previously that during the onset of effective cytotoxic antitumor responses, CD8$^+$ T cells establish stable, long-lasting contacts with antigen-presenting DCs (Hugues et al., 2006; Scholer et al., 2008). These stable interactions induce a strong arrest of CD8$^+$ T cells in tdLNs. We therefore decided to analyze in more detail the effect of Foxp3$^+$CD25$^+$ T cell inactivation or depletion on OTI T cell dynamics early (20 hr) after their adoptive transfer to tumor-bearing mice (Figures 2A–2C). We have shown previously that at this time point, OTI T cells arrested their migration in LNs draining immunogenic EL4 tumors expressing OVA (EG7 tumors) (Scholer et al., 2008). In order to analyze the dynamics of OTI T cell migration, we adoptively transferred CFP-expressing OTI T cells to Foxp3$^+$-EGFP mice. As shown in Figure 2, OTI T cell motility (mean velocity, confinement ratio, and arrest coefficient) was similar in LNs draining MCA-OVA tumors (Movie S1), in LNs draining MCA tumors that did not express OVA, or in LNs in the absence of tumors. Therefore, OVA-expressing MCA tumors, in contrast to EG7 tumors (which were rejected even in the presence of Foxp3$^+$ T cells [Scholer et al., 2008]), did not affect OTI T cell motility in tdLNs, consistent with the absence of effective antitumor immune responses and tumor rejection in these mice.

In contrast, Foxp3$^+$CD25$^+$ T cell inactivation by the anti-CD25 antibody induced a marked arrest in OTI T cell motility, in the MCA-OVA-draining LNs (Figures 2A–2C; Movie S2). The mean velocity dropped from 6.8 ± 3.3 μm/min to 3.6 ± 2.6 μm/min ($p < 0.0001$), and the confinement ratio decreased from 0.6 ± 0.22 to 0.44 ± 0.21 ($p < 0.0001$). The arrest coefficient, in contrast, increased from 19% ± 24% to 45% ± 29% ($p < 0.0001$). This change in OTI T cell motility was not observed in the popliteal LNs (ndLNs) of the same animals (Figure S2A) or in the axillary LNs of animals bearing MCA tumors that did not express OVA (Figure 2B).

We previously have shown that stable T-DC interactions correlate with efficient CD8$^+$ T cell priming (Hugues et al., 2004; Scholer et al., 2008). Therefore, we investigated the effect of Foxp3$^+$CD25$^+$ T cell inhibition on OTI T cell priming. To do so, we adoptively transferred OTI T cells 10 days after tumor inoculation to mice treated or not treated with anti-CD25 and analyzed OTI T cell activation, proliferation, and differentiation. Foxp3$^+$CD25$^+$ T cell inactivation did not affect CD69 expression or the rate of division of the transferred OTI T cells (Figures S2B and S2C). Treatment with anti-CD25 antibody, in contrast, favored OTI T cell accumulation and increased the production of IFN-γ in tdLNs (Figures S2D and S2E). We concluded that the decreased motility of OTI cells observed upon Treg cell inactivation correlates with more efficient priming (increased T cell numbers and IFN-γ production).

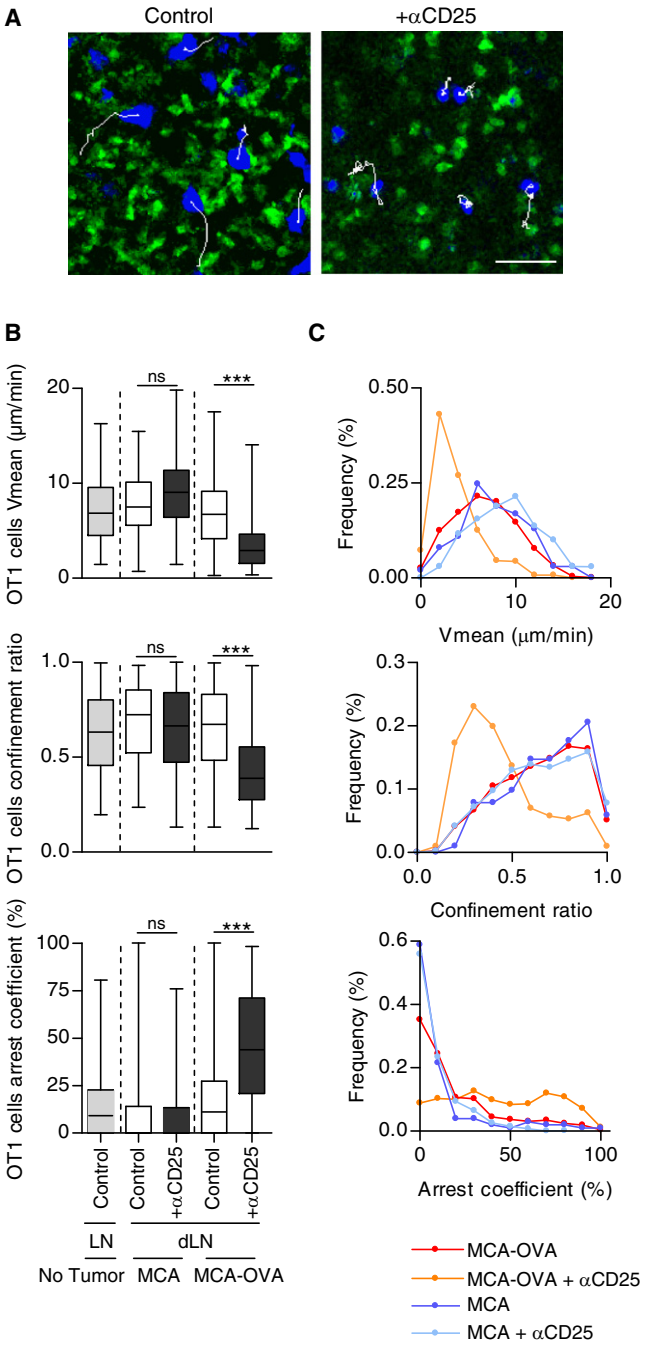

Figure 2. Foxp3+ CD25+ T Cells Inhibit CD8+ T Cells Arrest during Priming in Tumor-Draining Lymph Nodes

Twenty hours after adoptive transfer of CFP-expressing OTI T cells in tumor-bearing or tumor-free Foxp3-EGFP mice, OTI T cell motility was analyzed by two-photon imaging in explanted LNs as indicated.

(A) Time-lapse two-photon microscopy images. OTI T cells are shown in blue, Foxp3+ T cells shown in green; and the white bar represents 35 μm. Typical OTI T cell track paths are represented (white lines).

(B) OTI T cells were individually tracked and the mean velocity (upper panel), the confinement ratio (middle panel), and the arrest coefficient (lower panel) were determined. The box extends from the 25th to the 75th percentile, the line at the middle is the median and the error bars extend from the lowest up to the highest values. Graphs represent pooled data from at least three independent experiments. n = 180 OTI T cells for draining lymph nodes (dLNs) of tumor-free mice; n = 169 for draining lymph nodes of MCA-bearing mice; n = 863 for draining lymph nodes of MCA-OVA-bearing mice with anti-CD25; n = 777 for draining lymph nodes of MCA-OVA-bearing mice, and n = 416 for draining lymph nodes of MCA-OVA-bearing mice with anti-CD25.

(C) Distribution of OTI T cells as a function of their mean velocity (higher panel), confinement ratio (middle panel), and coefficient arrest (lower panel) in the draining lymph node of MCA-OVA-bearing mice treated (orange) or not treated (red) with anti-CD25 or in the draining lymph node of MCA-bearing mice treated (light blue) or not treated with anti-CD25 (dark blue).

For confirmation of these observations in another experimental model, Foxp3+ T cells were genetically depleted with diphteria toxin (DTx) in mice expressing the DTx receptor under the control of the Foxp3 promoter (DEREG mice, Lahl et al., 2007). As described previously, Foxp3+ T cells were fully depleted after two consecutive injections of DTx (Figure S3A). As the reappearance of emigrating Foxp3+ T cells occurred within 4 to 5 days, depletion was maintained by DTx treatment every 4 days. During the period of tumor growth, no mortality was observed.

Foxp3+ T cell depletion in DEREG mice also induced effective tumor rejection (Figure S3B) and OTI T cell motility in the tdLNs was reduced, but not as strongly as after PC61 treatment (Figure S4C). This difference could reflect the fact that in these mice, OTI T cells were more clustered and distributed closer to the subcapsular area, as compared to control LNs (not shown). It is noteworthy that we observed some slight differences in OTI T cell motility between DEREG mice and littermate controls in the absence of DTx treatment, suggesting a basal transgene effect. In addition, the proliferation rate and the production of IFN-γ by OTI T cells were both increased after treatment with DTx, as compared to treated littermates (Figures S3D and S3E).

We conclude that Foxp3+CD25+ T cell inactivation (with anti-CD25 antibodies) or depletion (with DTx) enhanced OTI T cell priming in mice bearing MCA-OVA tumors.

Foxp3+CD25+ T Cells Control the Number of DCs in Tumor-Draining Lymph Nodes

By presenting antigen to T cells, DCs determine their motility in lymph nodes. T cell arrests depend on several parameters, including the density of antigen-presenting DCs, their maturation state, and the amounts of antigen presented on the DCs (Celli et al., 2007; Hugues et al., 2004; Scholer et al., 2008). The effect of Foxp3+CD25+ T cell inactivation on CD8+ T cell motility could therefore be due to a modulation of DC functions by Foxp3+CD25+ T cells. Given that several studies reported that Foxp3+ T cells can modify DC maturation in vitro (Cederbom et al., 2000; Lewkowich et al., 2005; Misra et al., 2004), we first analyzed the maturation profile of the DCs in tdLNs, 10 days after tumor inoculation in anti-CD25 treated or untreated mice (in the absence of OTI T cell transfer). As shown in Figure 3A, the surface expression of CD80, ICAM-1, I-Ab, and CD40 on DCs was not modified by the anti-CD25 treatment. Similar results were observed in DEREG mice (not shown). These results, however, do not exclude the possibility that Foxp3+ T cells affect maturation in a subpopulation of DCs, which we may have missed in this global FACS analysis.

In contrast, we observed a clear increase in both the percentage and the absolute numbers of CD11chi cells in tdLNs

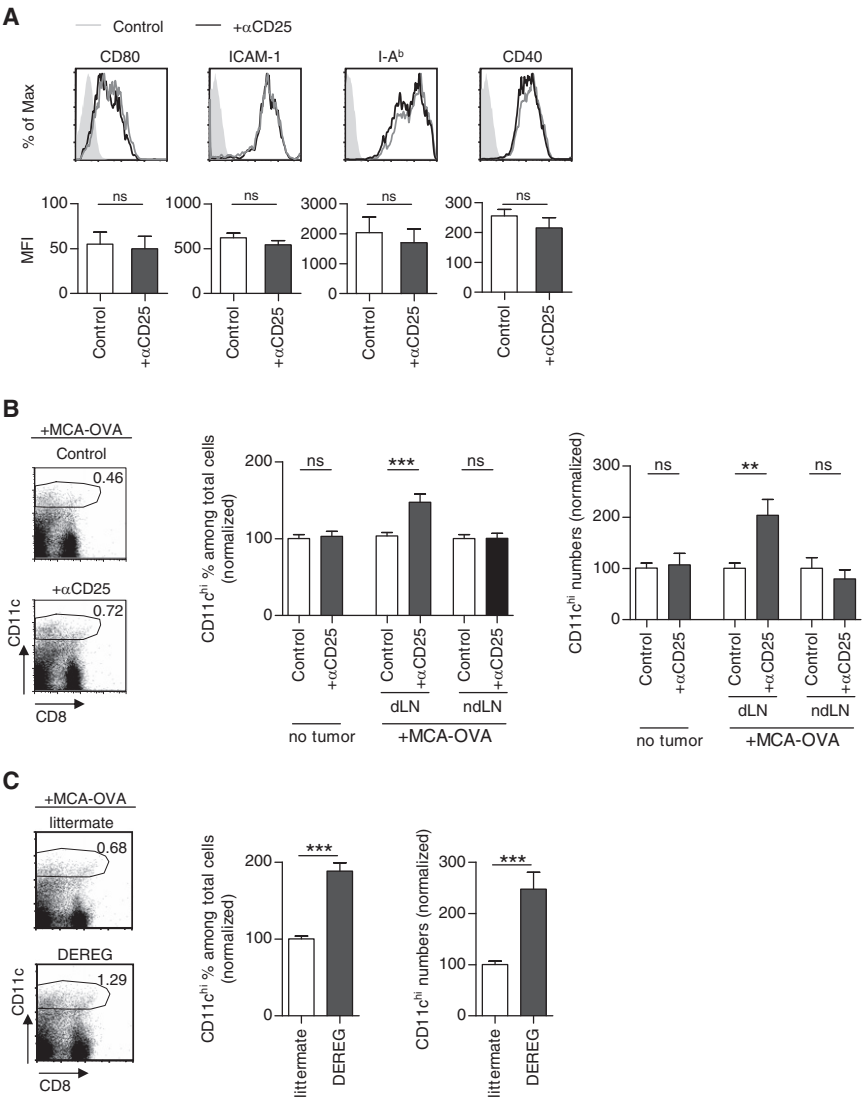

Figure 3. Foxp3+ CD25+ T Cells Limit DC Numbers in Tumor-Draining Lymph Nodes

Ten days after tumor inoculation, DC maturation profile and numbers were determined in tdLNs of mice treated or not treated with anti-CD25.

(A) Surface expression of CD80, ICAM-1, I-A^b, and CD40 were analyzed by flow cytometry after gating on $CD11c^{hi}$ population. Histograms represent expression profiles of these maturation markers (full histograms are isotype controls). Graphs represent the mean fluorescence intensity of these maturation markers (data are pooled from three independent experiments). Each bar represents a mean ± SD.

(B) Quantification of DC percentage in lymph nodes by flow cytometry. Representative dot plots of $CD11c^{hi}$ population in tumor-draining lymph nodes of mice treated or not treated with anti-CD25 (left panel). $CD11c^{hi}$ percentage (middle panel) and number (right panel) in lymph nodes of tumor-free mice and in draining lymph nodes (dLNs) and nondraining lymph nodes (ndLNs) of tumor-bearing mice are shown. For comparison of the percentages and numbers of $CD11c^{hi}$ cells in several experiments, the results were normalized and plotted as a percentage (as described in the material and methods). Bars represent mean ± SD of different mice from three to eight independent experiments.

(C) Quantification of DC percentage in lymph nodes by flow cytometry. Representative dot plots of $CD11c^{hi}$ population in tumor-draining lymph nodes of littermate and DEREG (left panel). Increase percentage and number of $CD11c^{hi}$ cells in DEREG mice and littermate after DTx treatment were normalized as in (B). For all conditions raw mean ± SD of DC percentages and numbers are indicated in Figure S4.

of anti-CD25-treated mice, as compared to untreated mice (of 50% and 100%, respectively) (Figure 3B and Figures S4A–S4D). These cells were also $CD11b^+$ and I-$A^{b\ hi}$, suggesting a myeloid origin (not shown). Accumulation of $CD8^-$ and $CD8^+$ DCs was similarly modified by the anti-CD25 treatment. This increase in the percentage and the absolute numbers of $CD11c^{hi}$ cells upon injection of anti-CD25 was neither observed in nondraining LNs nor in tumor-free mice. Similar accumulation of DCs was observed in tumor-bearing DEREG mice after $Foxp3^+$ T cell depletion (Figure 3C and Figures S4B–S4D). We conclude that $Foxp3^+CD25^+$ T cells reduce the density of the endogenous DC-network in tumor-draining lymph nodes. These results suggest that tumor-activated $Foxp3^+$ T cells modulate the recruitment, the retention, and/or the viability of DCs in tdLNs.

Imaging of DC Death in Tumor-Draining Lymph Nodes

$Foxp3^+$ T cells were previously shown to be cytotoxic in several experimental models (Cao et al., 2007; Grossman et al., 2004; Janssens et al., 2003; Zhao et al., 2006). We therefore analyzed the possibility that $Foxp3^+$ T cells control the viability of DCs in tdLNs. We were unable to detect any difference in the viability of DCs in tdLN of mice treated or not treated with anti-CD25 using annexin V staining ex vivo (not shown). Because dying cells are rapidly eliminated by phagocytosis in vivo and can be lost during LN dissociation, we decided to further investigate this point by using real-time imaging. We used an assay for in vivo cytotoxicity previously described (Mempel et al., 2006). In vitro-generated DCs were labeled with Hoechst (nuclear labeling) and 5μM 5-(and-6)-(((4-chloromethyl)benzoyl)amino)tetramethylrhodamine (CMTMR, cytosolic labeling). DCs that lose their cytosolic red CMTMR labeling when the plasma membrane becomes permeable, while maintaining their nuclear blue Hoechst labeling, and stopped moving were scored as "dying DCs" (see Figure 4A and Movie S3).

In order to evaluate their survival after adoptive transfer to MCA-OVA bearing mice, we transferred DCs loaded with the I-A^b restricted $OVA_{323-339}$ peptide to $Foxp3^+$-EGFP mice bearing MCA-OVA tumors. The survival of the transferred DCs was analyzed 18–24 hr later with two-photon dynamic microscopy in the T cell zones (100–200 μm deep) in explanted LNs. The

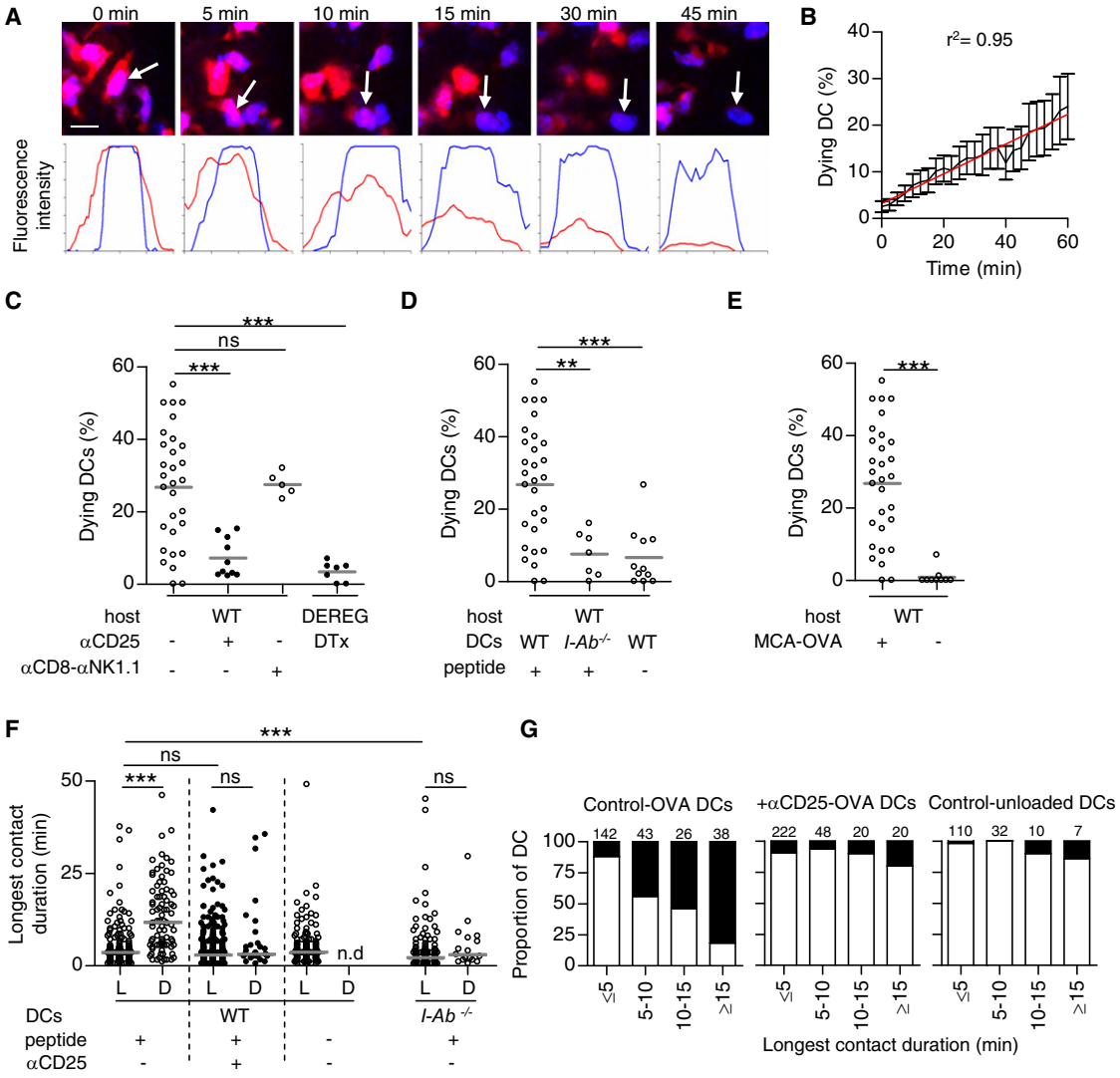

Figure 4. In Vivo Imaging of Foxp3+ T Cell-Mediated DC Death

Bone marrow-derived DCs were labeled with Hoechst (blue) and CMTMR (red) and injected s.c. 9 days after tumor inoculation in Foxp3-EGFP mice bearing or not bearing a tumor. Mice were treated or not treated, as indicated, with anti-CD25 2 days after tumor inoculation. Tumor-draining lymph nodes were imaged with two-photon microscopy 24 hours after DC adoptive transfer.

(A) Time-lapse two-photon microscopy images. Example of DC-death visualization 36 × 36 μm (white bar represent 10 μm). Histograms represent line-scan analysis of the fluorescence intensity emitted by Hoechst (blue line) or CMTMR staining (red line) of the indicated DC along time (lower panel).

(B) Rate of DC death along time. Transferred DCs were loaded with $OVA_{323-339}$ peptide (1 μM) and injected in WT tumor-bearing mice. The graph represents the mean ± SEM percentage of dying DCs along time from 11 movies from 6 independent experiments.

(C–E) Percentage of dying DCs observed in different experimental conditions as indicated. Each dot represents the percentage of dying DCs in a single movie (10–100 DCs were analyzed per movie). As shown in (C), transferred DCs were loaded with $OVA_{323-339}$ peptide (1 μM) and injected in tumor-bearing mice treated as indicated. As shown in (D), WT or *I-Ab*$^{-/-}$ DCs loaded or not loaded with $OVA_{323-339}$ peptide were injected as indicated in tumor-bearing mice. As shown in (E), transferred DCs were loaded with $OVA_{323-339}$ peptide and injected into mice bearing a tumor or not. Gray bars represent the median of the percentages of dying DCs out of two to ten independent experiments.

(F) Longest contact duration between Foxp3+ T cells and DCs are represented for DCs that are going to die or remain alive during the imaging period: living (L) versus dead (D). Each dot represents one DC. Bars represent the medians.

(G) Frequency of DC death as a function of the longest Foxp3+ T cell-DC contact duration. Bars represent the proportion of living (white) and dying (black) DCs. DCs were loaded or not loaded with $OVA_{323-339}$ peptide (1 μM) and injected in mice treated or not treated with anti-CD25, as indicated. Numbers above the bars indicate the numbers of cells analyzed.

proportion of dying DCs in the 1-hr-long movies was quite variable, ranging from 0% to more than 55% of the DCs in each imaging field, with a constant rate over time (Figure 4B). In more than 30 movies, from over ten independent experiments, an average of 27% ±16% of the DCs in each field were found to die during the imaging period (Figure 4C). In order to address the possibility that Foxp3+CD25+ T cells control DC viability in tdLNs, we treated the animals with anti-CD25 before DC

adoptive transfer. Alternatively, we depleted Foxp3$^+$ T cells by using DTx in DEREG mice. The inactivation of Foxp3$^+$CD25$^+$ T cells by anti-CD25 or Foxp3$^+$ T cell depletion by DTx both strongly decreased the proportions of dying DCs (Figure 4C, Movies S4 and S5), indicating that DC death in tdLNs is Foxp3$^+$ CD25$^+$ T cell dependent. We observed large autofluorescent cells in tdLNs from anti-CD25- and DTx-treated mice (Movie S5 and data not shown), and such cells may represent macrophages that have phagocytosed dying Foxp3$^+$ T cells.

Both CD8$^+$ T cells (Guarda et al., 2007) and NK cells (Yu et al., 2006) were shown previously to kill DCs under different conditions. To investigate the potential involvement of these two cell types in the DC death observed in tumor-bearing mice, we depleted these two cell populations by treating tumor-bearing mice with anti-CD8 and anti-NK1.1 before the adoptive transfer of the DCs. As shown in Figure 4C, CD8$^+$ T cell and NK cell depletion did not affect DC death in tdLNs. We conclude that Foxp3$^+$ T cells can modulate the survival of DCs in tdLNs.

The requirements for the control of DC viability by Foxp3$^+$ T cells in tdLNs were further characterized. Only few DCs died when they were not loaded with the $OVA_{323-339}$ peptide or were deficient for MHC class II molecules (respectively 7.6% and 6.6% dying DCs) (Figure 4D). Likewise, no significant DC death was observed when $OVA_{323-339}$ peptide loaded DCs were adoptively transferred to tumor-free mice (Figure 4E).

Phototoxic effects due to DC labeling (Hoechst and CMTMR) and laser-light exposure might induce DC death and thus interfere with our quantification. Arguing against this possibility, we first showed that the rate of DC death is constant over time (Figure 4B) and, secondly, it is very unlikely that this phototoxic effect happens only in a single experimental condition (for class II MHC-sufficient DCs, loaded with the $OVA_{323-339}$ peptide and transferred into tumor-bearing mice in the presence of fully functional Foxp3$^+$ T cells). Moreover, we quantified DC death without any prior continuous light exposure, by taking single-shot images of randomly chosen fields from tdLNs. Again, DC death was higher when DCs were loaded with the $OVA_{323-339}$ peptide, as compared to unloaded DCs (39% ±23% versus 18% ± 11%, respectively, $p < 0.0001$) (Figure S5A) showing antigen-dependent DC death in the absence of prolonged exposure to laser light.

We conclude that the control of DC viability by Foxp3$^+$ T cells is MHC class II restricted and antigen dependent and requires the presence of a tumor.

Analysis of DC-Foxp3$^+$ T Cell Interactions in Tumor-Draining Lymph Nodes

In order to further investigate the role of Foxp3$^+$ T cells in DC death in tdLNs, we analyzed the dynamic interactions between these two cell types. To do so, we imaged polyclonal Foxp3$^+$ T cells in Foxp3-EGFP mice after adoptive transfer of labeled DCs. In many cases, we observed death of DCs while they were interacting tightly with one or more Foxp3$^+$ T cells (Movie S6). In order to quantify these interactions, we defined three parameters that quantify the interactions of each DC with Foxp3$^+$ T cells: (1) the frequency of contacts (interaction number/hour, represents the number of contacts that each DC establishes with Foxp3$^+$ T cells, normalized to the density of Foxp3$^+$ T cells in each movie), (2) the cumulative contact duration (addition of the durations of all the individual contacts established by a DC with Foxp3$^+$ T cells during 1 hr, normalized to the density of Foxp3$^+$ T cells in each movie), and (3) the duration of the longest contact with a Foxp3$^+$ T cell for each DC.

These parameters were similar in untreated and anti-CD25-treated animals, and when DCs were sensitized or not sensitized with $OVA_{323-339}$ peptide. In contrast, in the absence of MHC class II expression on the DCs, all three parameters were significantly reduced. The reduction in the frequency of contacts between Foxp3$^+$ T cells may reflect a reduction in the contact duration, given that contacts shorter than 30 s (the interval of our imaging) can be missed. These results indicate that contacts between DCs and Foxp3$^+$ T cells in tdLNs are dependent on class II MHC expression on DCs.

In order to further investigate the possible relationship between the observed DC-Foxp3$^+$ T cell contacts and DC death, we analyzed separately the DCs that were going to die and those that remained alive during each movie. The different parameters described above were quantified in each of the two groups. Figure 4F and Figure S5B show that the frequency of the Foxp3$^+$ T cell-DC contacts was not different between the DCs that were going to die and those that remained alive. In contrast, the DCs that were going to die established longer contacts with Foxp3$^+$ T cells than those that remained alive, as outlined both by the cumulative contact duration (mean of 13.4 ± 13.2 min for living DCs versus 23.4 ± 22 min for dying DCs, $p < 0.0001$) (Figure S5B) and the longest contact duration (mean of 5.1 ± 5.9 min for living DCs versus 13.4 ± 9.6 min for dying DCs, $p < 0.0001$) (Figure 4F). These long lasting contacts of Foxp3$^+$ T cells with DCs that were going to die were not observed with DCs that did not express MHC class II molecules.

The analysis of the proportion of dying DCs as a function of the duration of the longest contact showed that DCs that established longer contacts with Foxp3$^+$ T cells had a higher probability to die than DCs that established shorter contacts (more than 80% of the DCs that establish contacts longer than 15 min with Foxp3$^+$ T cell died during the movies, whereas only less than 10% of the DCs that established contacts shorter than 5 min do so, Figure 4G). These results establish a direct relationship between the duration of the DC-Foxp3$^+$ T cell contacts and the death of the DCs. The results also exclude the possibility that DC death is due to phototoxicity during the movies, given that there is no reason that phototoxic death affects selectively DCs that interact more stably with Foxp3$^+$ T cells. In addition, we did not observe long-lasting contacts that started with DCs already dead, indicating that Foxp3$^+$ T cells do not adhere "nonspecifically" to dying cells. Individual representative examples of Foxp3$^+$ T cells-DC interactions along time are shown in Figure S5C. The vast majority of the Foxp3$^+$ T cell-DC interactions started before the CMTMR labeling started decreasing. These observations show a correlation between long-lasting contacts with Foxp3$^+$ T cell and DC death, suggesting that the long-lasting contacts are a cause, rather than a consequence, of DC death. We conclude that Foxp3$^+$ T cell-dependent DC death involves direct contacts between these two cell types.

Foxp3$^+$CD25$^+$ T Cell-Mediated DC Death Is Perforin Dependent

Foxp3$^+$ T cells were previously shown to express perforin and granzyme B and to kill target cells under different experimental

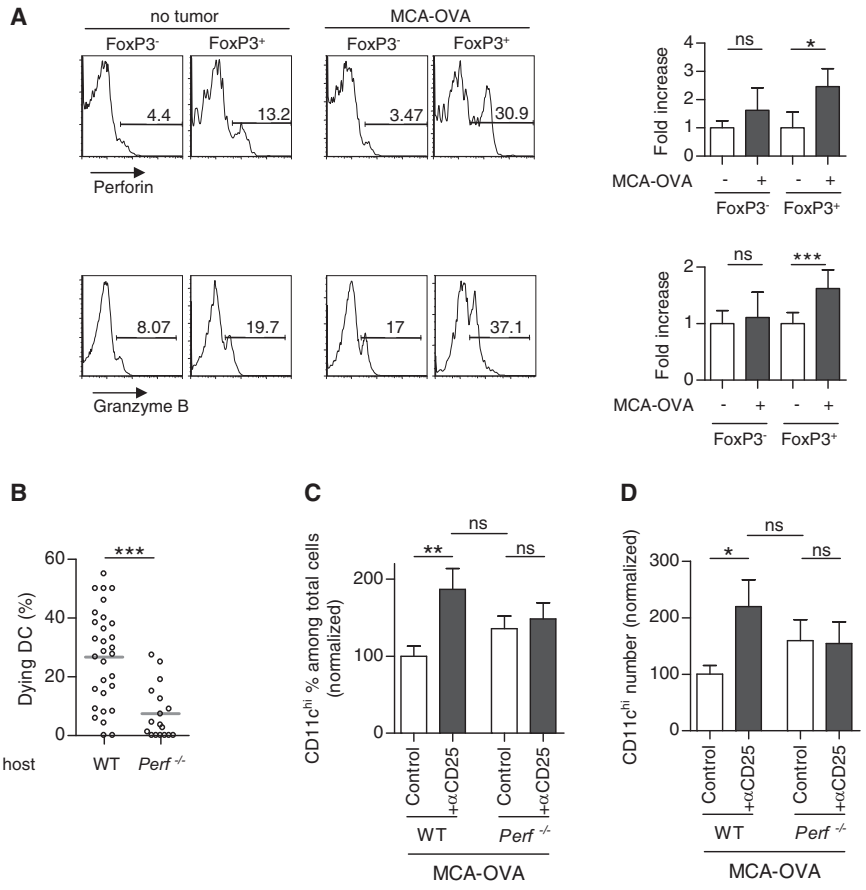

Figure 5. DC Death Is Dependent on Perforin Expression by Foxp3+ T Cells

(A) Representative histogram plot of perforin and granzyme B expression in $CD4^+Foxp3^-$ and $CD4^+Foxp3^+$ T cells from either tumor-bearing or tumor-free mice. Histogram bars represent the quantification of perforin and granzyme B expression in tumor-bearing mice, as a fold increase compared to the expression in tumor-free mice. Values represent a mean ± SD of six mice from two to three independent experiments.

(B) Quantification by two-photon imaging of DC death in WT and *Perf*$^{-/-}$ tumor-bearing mice. Transferred WT DCs were loaded with $OVA_{323-339}$ peptide.

(C and D) $CD11c^{hi}$ percentage (C) and number (D) in lymph nodes of *Perf*$^{-/-}$ and littermate tumor-bearing mice as determined by flow cytometry. Data were normalized as described in Figure 3. Bars represent medians of at least ten mice from five independent experiments. For all conditions raw mean ± SD of DC percentages and numbers are indicated in Figure S4.

conditions (Cao et al., 2007; Gondek et al., 2005; Grossman et al., 2004; McHugh et al., 2002; Zhao et al., 2006). We therefore tested the possibility that the $Foxp3^+CD25^+$ T cell-mediated DC death observed above is perforin dependent. We first analyzed the expression of perforin and granzyme B in $Foxp3^+$ T cells from tumor-free and tumor-bearing animals. As shown in Figure 5A, in tumor-free mice, a significant proportion of $Foxp3^+$ T cells (~13%) expressed perforin, whereas granzyme B was found in almost 20% of the cells. The proportion of $CD4^+Foxp3^-$ T cells expressing these two markers was much lower (~4% and 8%, respectively). In tumor-bearing mice, the respective proportions of perforin$^+$ and granzyme B^+ in $CD4^+$ $Foxp3^+$ T cells was significantly increased as compared to tumor-free animals, but not significantly in $CD4^+Foxp3^-$ T cells (Figure 5A). Given that more than 90% of $CD4^+Foxp3^+$ cells are also $CD25^+$, we can conclude that perforin$^+$ and granzyme B^+ $Foxp3^+$ T cells are mainly $CD25^+$.

To address the potential role of perforin in $Foxp3^+$ T cell-mediated DC death, we adoptively transferred WT DCs to perforin-deficient tumor-bearing mice. As shown in Figure 5B, DC death was strongly reduced in perforin-deficient mice, showing that DC death required perforin expression. The lack of DC death was not due to reduced $Foxp3^+$ T cell numbers or activation, which were both normal in perforin-deficient mice (not shown).

One prediction of these results is that the increase in DC numbers that we observed after inactivation of $Foxp3^+$ T cells in tumor-bearing mice should also be perforin dependent. To test this possibility, we analyzed the percentages and absolute numbers of DCs in the tdLNs of perforin-deficient mice and in their perforin-sufficient littermates. As shown in Figures 5C and 5D and Figure S4C and S4D, both the percentages and the absolute numbers of $CD11c^{hi}$ cells were increased in perforin-sufficient littermates, but not in perforin-deficient mice after anti-CD25 treatment. We conclude that the $Foxp3^+CD25^+$ T cell-dependent decrease in the numbers of DCs in tdLNs is also perforin dependent.

The Adoptive Transfer of OTII Foxp3+ T Cell to Perforin-Deficient Mice Reconstitutes DC Death

To investigate whether $Foxp3^+$ T cells can kill DCs directly, we performed an in vitro cytotoxicity assay using activated OVA-specific (OTII) $Foxp3^+$ and OTII $Foxp3^-$ T cells. The $Foxp3^+$ OTII cells expressed greater amounts of perforin and granzyme than the $Foxp3^-$ OTII cells (Figure 6A). The target DCs were isolated from draining LNs of tumor-bearing or control mice and labeled separately with two different concentrations of CFSE, one of the two being also loaded with the $OVA_{323-339}$ peptide. After incubation with T cells, the proportion of CFSE high and low target DCs was analyzed by flow cytometry. As shown in Figure 6B, the $Foxp3^+$ OTII cells killed LN DCs from both tumor-bearing and control mice more efficiently that $Foxp3^-$ OTII cells.

In order to determine whether $Foxp3^+$ T cell-mediated cytotoxicity also occurred in vivo, we adoptively transferred OTII $Foxp3^+$, OTII $Foxp3^-$, and HY-specific (Marilyn) $Foxp3^+$ T cells to perforin-deficient animals (in which we failed to see any DC cytotoxicity, see Figure 5B). As shown in Figure 6C and in Movie S7, the injection of OTII $Foxp3^+$ T cells, but not of OTII $Foxp3^-$ or Marilyn $Foxp3^+$ T cells (specific for HY antigen and not OVA), reconstituted the death of adoptively transferred peptide-loaded

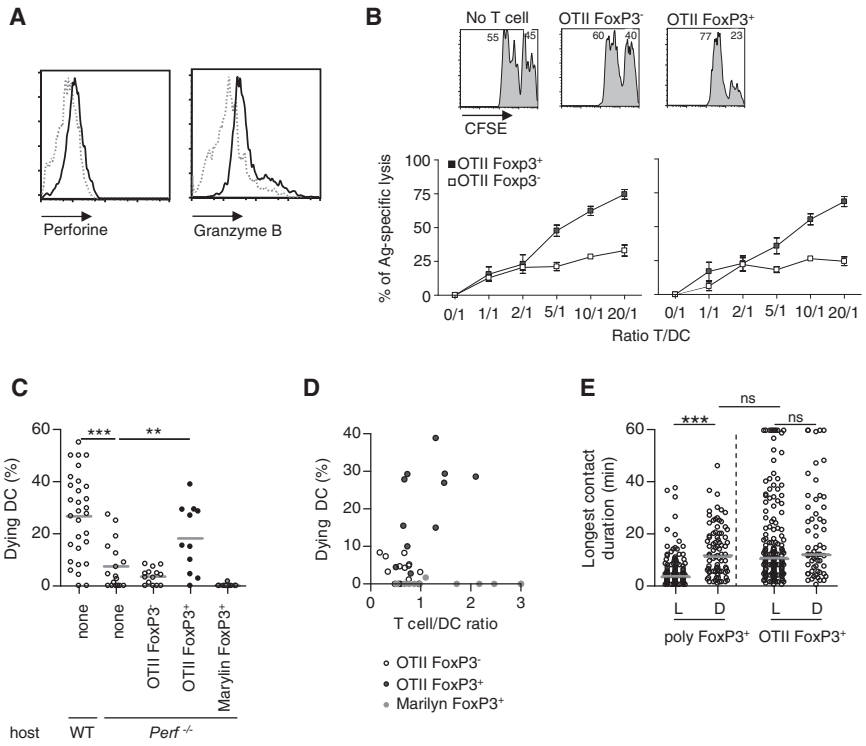

Figure 6. Cytotoxic OTII-Foxp3+ Cells Induce DC Death In Vivo

(A) Representative histogram plot of perforin and granzyme B expression on OTII Foxp3+ (black) and OTII Foxp3− (grey dashed) cells after 20 hr of coculture with $OVA_{323-339}$-loaded DCs.

(B) In vitro cytotoxicity assay by CFSE staining of DCs loaded with $OVA_{323-339}$ ($CFSE^{hi}$) or not ($CFSE^{lo}$), isolated from tdLNs (left panel) and LNs of tumor-free mice (right panel) in the presence of in vitro-expanded OTII Foxp3+ cells (black) and OTII Foxp3− cells (white). A representative histogram plot for 20/1 T/DC ratio with percentage of each population is shown. Graphs represent the mean ± SEM of triplicates from two independent experiments (lower panels).

(C) Quantification by two-photon imaging of DC death in WT and *Perf*$^{-/-}$ tumor-bearing mice reconstituted or not reconstituted with OTII Foxp3+ or Foxp3− or Marilyn Foxp3+ T cells as indicated.

(D) Distribution of the percentage of dying DCs as a function of the mean T cell/DC ratio in each imaging field.

(E) Longest contact duration between living or dying DCs and polyclonal (poly Foxp3+) or OTII Foxp3+ T cells as indicated.

DCs in perforin-deficient mice. The frequency of the adoptively transferred OTII Foxp3+ T cells in these animals was much lower than that of endogenous Foxp3+ T cells. We were therefore able, in this case, to analyze the proportion of dying DCs as a function of the transferred T cells/DC ratio in each movie. As shown in Figure 6D, DC death was proportional to the transferred T cell/DC ratios (Spearman r = 0.58, *), indicating a role for the Foxp3+ T cells present in each movie on DC death, as opposed to a global effect of Foxp3+ T cells transfer on the tdLNs' environment. The analysis of OTII Foxp3+ T cell-DC interactions revealed that, in contrast to polyclonal Foxp3+ T cells, the duration of the longest contact for each DC was equally long (median of 12 minutes) between DCs that are going to die or to stay alive (Figure 6E). These contacts were as long as the ones between polyclonal Foxp3+ T cells and the peptide-bearing DCs dying during the movies, consistent with the possibility that the long-lasting contacts of DCs with polyclonal Treg cells are actually antigen specific. We conclude that the death of peptide-loaded DCs in vivo mediated by adoptively transferred Treg cells is antigen specific and perforin dependent.

DISCUSSION

We show here that the number of DCs in tdLNs increases after Foxp3+ T cell inactivation or depletion in perforin-sufficient but not in perforin-deficient animals. These results suggest that DCs bearing tumor antigens maybe a target for Foxp3+ T cell-mediated cytotoxicity in tdLNs. Using dynamic two-photon imaging on explanted tdLNs, we found that adoptive transfer of DCs expressing a model tumor antigen results in DC death only when perforin-sufficient Foxp3+ T cells are present in the mice. This antigen-specific cytotoxic activity was confirmed in vitro. Foxp3+CD25+ T cell inactivation or depletion in tumor-bearing animals resulted in a marked arrest in antitumor CD8+ T cell migration, increased T cell priming, and subsequent tumor rejection. These findings suggest a mechanism of inhibition of the priming of anti-tumor CD8+ T cells by Foxp3+ T cells: by inducing the death of the DCs that present high tumor-antigen densities, Foxp3+ T cells decrease the amount of antigen present in tdLNs, thereby preventing effective CD8+ T cell priming, in particular IFN-γ production. IFN-γ plays a key role in the rejection of many different tumors in mice (Blankenstein, 2005). We found that IFN-γR1-deficient mice failed to reject MCA101 tumors, even after the adoptive transfer of OTI cells and Treg cell inactivation, suggesting an important role of IFN-γ in our tumor model (unpublished data). Therefore, the downregulation of IFN-γ production by regulatory T cell is most likely critical for tumor rejection.

A central question raised by our results is whether Foxp3+ T cells kill DCs directly or determine their survival indirectly. The first condition for the "direct killing" model is that DC death should be the consequence of a direct contact with Foxp3+ T cells. In vitro, we show that activated Foxp3+ OTII T cells are able to efficiently eliminate $OVA_{323-339}$-loaded LN DCs compared to Foxp3− OTII T cells. Our imaging results in vivo show a strong correlation between the duration of the contact and the death of the DCs: DCs that make contacts longer than 15 min with Foxp3+ T cells have a much higher probability to die than DCs that make brief contacts (80% of the DCs that made contacts longer than 15 min during the movies died). In both the absence of class II MHC OVA peptide and in class II MHC-deficient cells, the virtual absence of contacts longer than 15 minutes correlated with low DC death. Our results also show that the stable contacts are not a consequence of the

death of DCs, because: (1) we never observed a Foxp3$^+$ T cell establishing a contact longer that 15 min after DC death, and (2) the few dead DCs that were observed in the absence of peptide, or in anti-CD25-treated mice, did not establish long contacts with Foxp3$^+$ T cells.

These results, however, do not exclude that the observed stable interactions between living DCs and Foxp3$^+$ T cells correspond not to direct killing but, for example, to a putative Foxp3$^+$ T cell-mediated "help" of DC killing by other cytotoxic cells. Arguing against this possibility, our results showed that perforin expression in adoptively transferred OTII Foxp3$^+$, but not in OTII Foxp3$^-$, T cells is sufficient to cause DC death similar to the in vitro cytotoxicity assay. In addition, depletion of CD8$^+$ T and NK cells, the two main perforin-expressing cells, did not affect DC death in tdLNs. Altogether, these results strongly suggest a "direct killing" model. Foxp3$^+$ T cells have already been shown in several independent studies to display cytotoxic capacity (Cao et al., 2007; Grossman et al., 2004; Janssens et al., 2003; Zhao et al., 2006). Whether or not a particular tumor-dependent mode of activation of Foxp3$^+$ T cells is required to become cytotoxic in vivo needs further investigation.

One of the important characteristics of this study is that it was almost entirely realized with endogenous polyclonal Foxp3$^+$ T cells. Foxp3$^+$ T cell function was analyzed 10 days after tumor inoculation. At this point, the mice's immune system has been exposed to both the tumor and the tumor antigens, including OVA, during 10 days. We showed that this exposure resulted in a marked activation of both CD4$^+$Foxp3$^+$ and CD4$^+$Foxp3$^-$ T cells. Given that the cytotoxic effects that we have described are antigen dependent (only DCs presenting the OVA class II-MHC peptide died after adoptive transfer), the question of the antigen specificity of the Foxp3$^+$ T cells present in these tumor-bearing mice is relevant. It should be stressed here that the observation that the death of adoptively transferred DCs to tumor-bearing mice required the OVA peptide does not mean that the Foxp3$^+$ T cell response in the mice was restricted to this tumor antigen. Indeed, in the tumor-bearing mice, the T cells are exposed to a variety of tumor antigens, in addition to OVA, that are phagocytosed by DCs in an inflammatory environment. The adoptively transferred, in vitro-generated DCs have not been exposed to any other tumor antigen. The OVA class II MHC peptide used here was therefore the only "tumor" antigen present on these DCs. These results do not exclude that other "tumor" or self-antigens are recognized by Foxp3$^+$ T cells on DCs in vivo. It proved to be very difficult, however, in other experimental systems to demonstrate the antigen specificity of Foxp3$^+$ T cells ex vivo (Hsieh et al., 2006; Pacholczyk et al., 2007). It is most likely that among the large numbers of activated Foxp3$^+$ T cells, many of which are actively dividing (~30%, compared to 15% in tumor-free mice, as evidenced by their staining with KI67, data not shown), some are specific for tumor antigens, including OVA. Given that OVA is a non-self-antigen, it is also most likely that the polyclonal repertoire of Foxp3$^+$ T cells also includes this specificity.

Unfortunately, we failed to detect efficient cytotoxicity in vitro using the endogenous Foxp3$^+$ T cells. Indeed, significant cytotoxic activity is seen for a ratio of at least five OVA-specific Foxp3$^+$ T cell per DC. Reaching such ratios in vitro with endogenous Foxp3$^+$ T cells is probably not easy because of the likely low frequency of antigen-specific Foxp3$^+$ T cells.

Our findings identify a possible mode of regulation of CD8$^+$ T cell priming by Foxp3$^+$ T cells: by killing tumor antigen-presenting DCs in tdLNs, Foxp3$^+$ T cells limit the efficiency of T cell priming against tumor antigens. Whether this mode of regulation is specific for tumors or may represent a more general mechanism of Treg cell-mediated inhibition of immune responses will be addressed in future studies. Nevertheless, if Foxp3$^+$ T cells are also cytotoxic to tumor-antigen bearing DCs in humans, DC killing may contribute to limit the efficiency of DC-mediated vaccination in cancer patients.

EXPERIMENTAL PROCEDURES

Mice

C57BL/6 female mice were obtained from Charles River, (Les Oncins, France) and used between 6–10 weeks old. We crossed C57BL/6 *Rag2*$^{-/-}$ TCR (Vα2, Vβ5) transgenic mice (OTI) with UBI-GFP/BL6 or with the Actb-ECFP/BL6 to obtain the OTI-GFP and OTI-CFP mice, respectively (Boissonnas et al., 2007). B6-Foxp3^{tm1Mal} mice (called Foxp3-EGFP mice here) (Wang et al., 2008), DEREG mice (Lahl et al., 2007), perforin-deficient mice (Kägi et al., 1994), and Marilyn mice (Lantz et al., 2000) were described previously. We crossed Foxp3-EGFP mice with transgenic OTII mice to obtain OTII-Foxp3-EGFP mice. Live-animal experiments were done in accordance with the guidelines of the French Veterinary Department.

Cells

CD8$^+$ OTI T cells (specific for OVA$_{257-264}$ peptide in a H2-K^b context) were obtained from lymph nodes of OTI *Rag2*$^{-/-}$ (called OTI T cells here) mice (purity ~96%). Marilyn CD4$^+$ T cells were obtained from lymph nodes of Marilyn *Rag2*$^{-/-}$ mice and stained with 5 μM 5-(and-6)-(((4-chloromethyl)benzoyl)amino)tetramethylrhodamine (CMTMR, Invitrogen, Cergy Pontoise, France) in PBS during 10 min at 37°C. CD4$^+$ GFP$^+$ and CD4$^+$GFP$^-$ T cells were purified by flow cytometry and stimulated in vitro (in medium containing 2000 IU/Ml rhIL-2 (Chiron Corp), with LPS (1 μg/ml)-treated, OVA$_{323-339}$ peptide (1 μM)-pulsed, bone marrow-derived DCs. After 5 days, IL-2 supplemented medium was added to the culture. Cells were collected after 8–9 days. For the two-photon imaging experiments, bone marrow-derived DCs, differentiated as previously described (Naik et al., 2005), were loaded with 1 μM OVA$_{323-339}$ for 1 hr, washed, and labeled with 1 μM Hoechst in PBS during 10 min at 37°C before staining with 5 μM CMTMR in PBS during 10 min at 37°C. The cells were injected s.c. in the flank of tumor-bearing or tumor-free mice. The MCA101 (MCA) cell line was stably transfected with an control plasmid or a plasmid encoding for soluble Ovalbumin (OVA) for generation of the control MCA-Mock and MCA-OVA, respectively (Zeelenberg et al., 2008). All cell lines were cultured in DMEM (Gibco, Invitrogen, Cergy Pontoise, France) supplemented with antibiotics and 10% FCS.

In Vivo Tumor Growth and Cell Depletions

MCA-OVA cells were injected subcutaneously in the flank of mice and the tumor size was measured twice a week with a caliper, V = L × l × (L + l)/2. The same day, the mice were injected with 400 μg of anti-CD25 (PC61) or rat IgG1 isotype control (HRPN) (BioXcell, West Lebanon NH, USA). For imaging of DC death, PC61 was injected at day 2 after tumor inoculation. Serum quantification of Rat IgG was performed by ELISA (Bethyl, Montgomery, TX, USA). For DEREG mice and littermates, 1μg of DTx (Merck, Nottingham, UK) was injected intraperitoneally (i.p.) in PBS at days 3 and 4, at days 8–9, and at days 13–14 after tumor inoculation to induce and maintain Foxp3$^+$ T cell depletion. Ten days after tumor inoculation 5 × 10^6 naive OTI T cells were injected intravenously (i.v.) CD8$^+$ T cells and NK cells were depleted 24 hours before imaging; injecting i.p. 200 μg of both H35 and PK136 clones respectively.

Flow Cytometry

Phenotypic characterization of T cells was performed using a FACSCalibur (Becton Dickinson Franklin Lakes, NJ, USA). MCA-tumor, draining (axillary),

and nondraining (the 2 popliteal) lymph nodes were harvested at different days after tumor inoculation or adoptive transfer of naive OTI T cells. Cell suspensions were prepared in PBS 0.5% BSA, and cells were labeled regarding the experiment with anti-CD69-PerCPCy5.5 (clone H1.2F3), anti-CD62L-APC (clone MEL-14), anti-CD44-PE (clone IM-7), anti-CD8-APC (clone 53-6.7), anti-CD11b-PercP-Cy5.5 (clone M1/70), anti-CD11c-PE or -APC (clone HL3), anti-CD80-FITC (clone 16-10A1), anti-ICAM-1-FITC (clone 3E2), anti-CD40-PE (clone 3/23), and anti-I-A^b-PE (clone AF6-120.1) (BD Biosciences, San Jose, USA). Regulatory T cells were discriminated by labeling with anti-CD25-PercPCy5.5 (clone PC61), anti-CD4-APC (clone RM4-5, BD Biosciences, San Jose, USA) and for Foxp3 through GFP expression from Foxp3-EGFP mice. For intracellular cytokine staining, cell suspensions were incubated for 3 hr at 37°C in the presence of 5 μg/ml Brefeldin A, fixed in 2% PFA, and incubated in PBS 0.5% BSA with saponin at 0.1% in the presence of anti-IFN-γ-APC (clone XMG1.2). For anti-perforin-PE (Clinisciences, Montrouge, France), anti-Granzyme B-PE (clone GB12, Caltag, Invitrogen) and anti-Foxp3-APC (clone FJK-16s, Clinisciences, Montrouge, France) staining, fixation and permeabilization were performed with Foxp3 staining kit (Clinisciences) in accordance with the manufacturer's instructions. For CFSE experiments, CD45.1 OTI T cells were incubated for 10 min at 37°C in PBS with 5 μM CFSE (Molecular Probes, Invitrogen). A total of 5×10^6 cells were injected in PBS into CD45.2 tumor-bearing or tumor-free mice. After 4 or 6 days, CFSE dilution in axillary LNs was measured, while gating on CD45.1 (A20) $CD8^+$ T cells.

Two-Photon Laser-Scanning Microscopy

A total of 5×10^6 naive CFP-expressing OTI T cells were injected i.v. to Foxp3-EGFP tumor-bearing recipients. All imaging experiments were performed on explanted tissue. LNs were carefully collected and were immobilized in an imaging chamber perfused with oxygenated (95% O_2 plus 5% CO_2) RPMI medium containing 10% FCS. Local temperature was monitored and maintained at 37°C. Lymph node imaging was performed 24 hr after adoptive transfer. T cells could be detected up to 200 μm from the surface of LNs.

Measurements were performed in at least three independent experiments. The two-photon laser-scanning microscopy (TPLSM) setup used was an LSM510 Meta (Zeiss, Jena, Germany) coupled to a Maitai DeepSee femtosecond laser (690–1020 nm) (Spectra-Physics, Mountain View, CA, USA). Three fluorescence channels were recorded simultaneously with two dichroic mirrors (495 nm and 555 nm) in combination with 472/30 (CFP/Hoechst), 520/35 (GFP), and 585/40 (CMTMR) bandpass filters. The excitation wavelength was 850 nm. For analysis of cell migration, every 30s during 30–60 min, six consecutive 230 × 230 μm^2 images, with 6 μm *z* spacing with an 40 × 0.8w objective were taken. Images were average-projected with Image J software (NIH), and manual tracking of individual cells was performed with Metamorph software. The acquisition and analysis protocols for all experimental conditions to be compared were identical. The arrest coefficient is defined as the proportion of time each cell's instantaneous velocity (calculated for every 30 s interval) is lower than 2 μm/min. The confinement ratio corresponds to the ratio of the distance between the initial and the final positions of each cell to the total distance covered by the same cell. In all our quantifications, only direct contacts between corpses of $Foxp3^+$ T cells and DCs were taken into account. Putative distant contacts through dendrites were not considered. The overestimation of cell-to-cell contacts due to the z projections performed for the quantifications is most likely small (especially for long-lasting contacts) and is similar for all conditions. The interaction number/hour represent the number of new contact made by each DC with a $Foxp3^+$ T cell reported during 1 hr and normalized to the density of $Foxp3^+$ T cells in the field. Cumulated contact duration represents the cumulated duration of total contact made by each DC with $Foxp3^+$ T cells during 1 hr and normalized to the density of $Foxp3^+$ T cells in the field. The density of $Foxp3^+$ T cells was given by the mean of the number of $Foxp3^+$ T cells measured at different time points in the field reported to the volume of the field analyzed.

In Vitro Cytotoxic Assay

OTII T cells were cocultured for 20 hr with DCs isolated from tdLNs or LNs from tumor-free mice with anti-CD11c-magnetic beads (Miltenyi, Paris, France). For each condition, purified DCs were either loaded with 1 μM $OVA_{323-339}$ and labeled with 2 μM CFSE ($CFSE^{hi}$) or directly labeled with 0.2 μM CFSE ($CFSE^{lo}$). Percentages of antigen-specific lysis were calculated with the following formula:

$$\%\ \text{of antigen-specific lysis} = \left[1 - \left(\left(\%\ CFSE^{hi} / \%\ CFSE^{lo}\right) / \left(\%\ CFSE^{hi\ ctrl} / \%\ CFSE^{lo\ ctrl}\right)\right)\right] \times 100$$

Control corresponds to DCs cultured in absence of T cells.

Statistical Analysis and Normalization

Two-way ANOVA, student t tests, and Spearman correlation tests were performed for statistic experiments. For p values, *$p < 0.05$; **$p < 0.01$, ***$p < 0.001$, and "ns" is defined as not significant.

For each experiment, the mean percent or number of $CD11c^+$ cells in mice (three to five mice) from the control groups was calculated. The percent or number of $CD11c^+$ cells from each individual control and treated mouse was normalized to the mean of the control of the corresponding experiment (by dividing the value for each mouse—control and treated—by the mean of the control group and expressed as a percentage). The graphs presented in Figures 3B and 5C represent the mean of all the normalized values from all experiments obtained according to this procedure.

The statistical analysis of the nonnormalized results shown in Figures 3B, 3C, 5C, and 5D was performed with the two-way ANOVA test, as detailed in Figure S9.

SUPPLEMENTAL INFORMATION

Supplemental Information includes five figures and seven movies and can be found with this article online at doi:10.1016/j.immuni.2009.11.015.

ACKNOWLEDGMENTS

We would like to thank S. Krumeich and G. Sugano for experimental help, A. Trautmann, E. Donnadieu, M. Krummel, and R. Voituriez for helpful discussions, C. Thery and O. Lantz for critically reading the manuscript, and B. Salomon for providing the PC61 cell line. A.B. has been supported by Association pour la Recherche contre le Cancer (ARC) and Ligue contre le Cancer (LNCC); A.S. was a fellow of Ministère de l'Education et de la Recherche. The Foxp3-EGFP mice have been developed by the Plate-forme Technologique du Vivant IBISA. This work was supported by funding from Institut National de la Santé et de la Recherche Médicale; Centre National de la Recherche Scientifique; La Ligue Contre le Cancer; Association de la Recherche Contre le Cancer (ARC, Leopold Griffuel award); the Institut Curie; Fondation Bettencourt-Schueller; EC grant DC-Thera N°LSBH-CT-2004-512074 "Dendritic Cells for Novel Immunotherapies"; EC grant Cancer Immunotherapy LSHC-CT-2006-518234 "Cancer Immunology and Immunotherapy"; and EC grant ENCITE, Health-F5-2008-201842.

Received: May 11, 2009
Revised: October 14, 2009
Accepted: November 30, 2009
Published online: February 4, 2010

REFERENCES

Appay, V., Jandus, C., Voelter, V., Reynard, S., Coupland, S.E., Rimoldi, D., Lienard, D., Guillaume, P., Krieg, A.M., Cerottini, J.C., et al. (2006). New generation vaccine induces effective melanoma-specific CD8+ T cells in the circulation but not in the tumor site. J. Immunol. *177*, 1670–1678.

Blankenstein, T. (2005). The role of tumor stroma in the interaction between tumor and immune system. Curr. Opin. Immunol. *17*, 180–186.

Boissonnas, A., Fetler, L., Zeelenberg, I.S., Hugues, S., and Amigorena, S. (2007). In vivo imaging of cytotoxic T cell infiltration and elimination of a solid tumor. J. Exp. Med. *204*, 345–356.

Bopp, T., Becker, C., Klein, M., Klein-Hessling, S., Palmetshofer, A., Serfling, E., Heib, V., Becker, M., Kubach, J., Schmitt, S., et al. (2007). Cyclic adenosine

monophosphate is a key component of regulatory T cell-mediated suppression. J. Exp. Med. *204*, 1303–1310.

Cao, X., Cai, S.F., Fehniger, T.A., Song, J., Collins, L.I., Piwnica-Worms, D.R., and Ley, T.J. (2007). Granzyme B and perforin are important for regulatory T cell-mediated suppression of tumor clearance. Immunity *27*, 635–646.

Cederbom, L., Hall, H., and Ivars, F. (2000). CD4+CD25+ regulatory T cells down-regulate co-stimulatory molecules on antigen-presenting cells. Eur. J. Immunol. *30*, 1538–1543.

Celli, S., Lemaître, F., and Bousso, P. (2007). Real-time manipulation of T cell-dendritic cell interactions in vivo reveals the importance of prolonged contacts for CD4+ T cell activation. Immunity *27*, 625–634.

Chen, M.L., Pittet, M.J., Gorelik, L., Flavell, R.A., Weissleder, R., von Boehmer, H., and Khazaie, K. (2005). Regulatory T cells suppress tumor-specific CD8 T cell cytotoxicity through TGF-beta signals in vivo. Proc. Natl. Acad. Sci. USA *102*, 419–424.

Colombo, M.P., and Piconese, S. (2007). Regulatory-T-cell inhibition versus depletion: The right choice in cancer immunotherapy. Nat. Rev. Cancer *7*, 880–887.

Couper, K.N., Blount, D.G., de Souza, J.B., Suffia, I., Belkaid, Y., and Riley, E.M. (2007). Incomplete depletion and rapid regeneration of Foxp3+ regulatory T cells following anti-CD25 treatment in malaria-infected mice. J. Immunol. *178*, 4136–4146.

Gondek, D.C., Lu, L.F., Quezada, S.A., Sakaguchi, S., and Noelle, R.J. (2005). Cutting edge: Contact-mediated suppression by CD4+CD25+ regulatory cells involves a granzyme B-dependent, perforin-independent mechanism. J. Immunol. *174*, 1783–1786.

Green, E.A., Gorelik, L., McGregor, C.M., Tran, E.H., and Flavell, R.A. (2003). CD4+CD25+ T regulatory cells control anti-islet CD8+ T cells through TGF-beta-TGF-beta receptor interactions in type 1 diabetes. Proc. Natl. Acad. Sci. USA *100*, 10878–10883.

Grossman, W.J., Verbsky, J.W., Barchet, W., Colonna, M., Atkinson, J.P., and Ley, T.J. (2004). Human T regulatory cells can use the perforin pathway to cause autologous target cell death. Immunity *21*, 589–601.

Guarda, G., Hons, M., Soriano, S.F., Huang, A.Y., Polley, R., Martín-Fontecha, A., Stein, J.V., Germain, R.N., Lanzavecchia, A., and Sallusto, F. (2007). L-selectin-negative CCR7- effector and memory CD8+ T cells enter reactive lymph nodes and kill dendritic cells. Nat. Immunol. *8*, 743–752.

Hsieh, C.S., Liang, Y., Tyznik, A.J., Self, S.G., Liggitt, D., and Rudensky, A.Y. (2004). Recognition of the peripheral self by naturally arising CD25+ CD4+ T cell receptors. Immunity *21*, 267–277.

Hsieh, C.S., Zheng, Y., Liang, Y., Fontenot, J.D., and Rudensky, A.Y. (2006). An intersection between the self-reactive regulatory and nonregulatory T cell receptor repertoires. Nat. Immunol. *7*, 401–410.

Hugues, S., Fetler, L., Bonifaz, L., Helft, J., Amblard, F., and Amigorena, S. (2004). Distinct T cell dynamics in lymph nodes during the induction of tolerance and immunity. Nat. Immunol. *5*, 1235–1242.

Hugues, S., Boissonnas, A., Amigorena, S., and Fetler, L. (2006). The dynamics of dendritic cell-T cell interactions in priming and tolerance. Curr. Opin. Immunol. *18*, 491–495.

Janssens, W., Carlier, V., Wu, B., VanderElst, L., Jacquemin, M.G., and Saint-Remy, J.M. (2003). CD4+CD25+ T cells lyse antigen-presenting B cells by Fas-Fas ligand interaction in an epitope-specific manner. J. Immunol. *171*, 4604–4612.

Kägi, D., Ledermann, B., Bürki, K., Seiler, P., Odermatt, B., Olsen, K.J., Podack, E.R., Zinkernagel, R.M., and Hengartner, H. (1994). Cytotoxicity mediated by T cells and natural killer cells is greatly impaired in perforin-deficient mice. Nature *369*, 31–37.

Kohm, A.P., McMahon, J.S., Podojil, J.R., Begolka, W.S., DeGutes, M., Kasprowicz, D.J., Ziegler, S.F., and Miller, S.D. (2006). Cutting edge: Anti-CD25 monoclonal antibody injection results in the functional inactivation, not depletion, of CD4+CD25+ T regulatory cells. J. Immunol. *176*, 3301–3305.

Lahl, K., Loddenkemper, C., Drouin, C., Freyer, J., Arnason, J., Eberl, G., Hamann, A., Wagner, H., Huehn, J., and Sparwasser, T. (2007). Selective depletion of Foxp3+ regulatory T cells induces a scurfy-like disease. J. Exp. Med. *204*, 57–63.

Lantz, O., Grandjean, I., Matzinger, P., and Di Santo, J.P. (2000). Gamma chain required for naïve CD4+ T cell survival but not for antigen proliferation. Nat. Immunol. *1*, 54–58.

Lewkowich, I.P., Herman, N.S., Schleifer, K.W., Dance, M.P., Chen, B.L., Dienger, K.M., Sproles, A.A., Shah, J.S., Köhl, J., Belkaid, Y., and Wills-Karp, M. (2005). CD4+CD25+ T cells protect against experimentally induced asthma and alter pulmonary dendritic cell phenotype and function. J. Exp. Med. *202*, 1549–1561.

McHugh, R.S., Whitters, M.J., Piccirillo, C.A., Young, D.A., Shevach, E.M., Collins, M., and Byrne, M.C. (2002). CD4(+)CD25(+) immunoregulatory T cells: Gene expression analysis reveals a functional role for the glucocorticoid-induced TNF receptor. Immunity *16*, 311–323.

Mempel, T.R., Pittet, M.J., Khazaie, K., Weninger, W., Weissleder, R., von Boehmer, H., and von Andrian, U.H. (2006). Regulatory T cells reversibly suppress cytotoxic T cell function independent of effector differentiation. Immunity *25*, 129–141.

Miller, M.J., Safrina, O., Parker, I., and Cahalan, M.D. (2004). Imaging the single cell dynamics of CD4+ T cell activation by dendritic cells in lymph nodes. J. Exp. Med. *200*, 847–856.

Misra, N., Bayry, J., Lacroix-Desmazes, S., Kazatchkine, M.D., and Kaveri, S.V. (2004). Cutting edge: Human CD4+CD25+ T cells restrain the maturation and antigen-presenting function of dendritic cells. J. Immunol. *172*, 4676–4680.

Naik, S.H., Proietto, A.I., Wilson, N.S., Dakic, A., Schnorrer, P., Fuchsberger, M., Lahoud, M.H., O'Keeffe, M., Shao, Q.X., Chen, W.F., et al. (2005). Cutting edge: Generation of splenic CD8+ and CD8- dendritic cell equivalents in Fms-like tyrosine kinase 3 ligand bone marrow cultures. J. Immunol. *174*, 6592–6597.

North, R.J., and Bursuker, I. (1984). Generation and decay of the immune response to a progressive fibrosarcoma. I. Ly-1+2- suppressor T cells down-regulate the generation of Ly-1-2+ effector T cells. J. Exp. Med. *159*, 1295–1311.

Onizuka, S., Tawara, I., Shimizu, J., Sakaguchi, S., Fujita, T., and Nakayama, E. (1999). Tumor rejection by in vivo administration of anti-CD25 (interleukin-2 receptor alpha) monoclonal antibody. Cancer Res. *59*, 3128–3133.

Ostroukhova, M., Qi, Z., Oriss, T.B., Dixon-McCarthy, B., Ray, P., and Ray, A. (2006). Treg-mediated immunosuppression involves activation of the Notch-HES1 axis by membrane-bound TGF-beta. J. Clin. Invest. *116*, 996–1004.

Pacholczyk, R., Kern, J., Singh, N., Iwashima, M., Kraj, P., and Ignatowicz, L. (2007). Nonself-antigens are the cognate specificities of Foxp3+ regulatory T cells. Immunity *27*, 493–504.

Pandiyan, P., Zheng, L., Ishihara, S., Reed, J., and Lenardo, M.J. (2007). CD4+CD25+Foxp3+ regulatory T cells induce cytokine deprivation-mediated apoptosis of effector CD4+ T cells. Nat. Immunol. *8*, 1353–1362.

Scholer, A., Hugues, S., Boissonnas, A., Fetler, L., and Amigorena, S. (2008). Intercellular adhesion molecule-1-dependent stable interactions between T cells and dendritic cells determine CD8+ T cell memory. Immunity *28*, 258–270.

Skokos, D., Shakhar, G., Varma, R., Waite, J.C., Cameron, T.O., Lindquist, R.L., Schwickert, T., Nussenzweig, M.C., and Dustin, M.L. (2007). Peptide-MHC potency governs dynamic interactions between T cells and dendritic cells in lymph nodes. Nat. Immunol. *8*, 835–844.

Somasundaram, R., Jacob, L., Swoboda, R., Caputo, L., Song, H., Basak, S., Monos, D., Peritt, D., Marincola, F., Cai, D., et al. (2002). Inhibition of cytolytic T lymphocyte proliferation by autologous CD4+/CD25+ regulatory T cells in a colorectal carcinoma patient is mediated by transforming growth factor-beta. Cancer Res. *62*, 5267–5272.

Tadokoro, C.E., Shakhar, G., Shen, S., Ding, Y., Lino, A.C., Maraver, A., Lafaille, J.J., and Dustin, M.L. (2006). Regulatory T cells inhibit stable contacts between CD4+ T cells and dendritic cells in vivo. J. Exp. Med. *203*, 505–511.

Tang, Q., Adams, J.Y., Tooley, A.J., Bi, M., Fife, B.T., Serra, P., Santamaria, P., Locksley, R.M., Krummel, M.F., and Bluestone, J.A. (2006). Visualizing

regulatory T cell control of autoimmune responses in nonobese diabetic mice. Nat. Immunol. *7*, 83–92.

Wang, H.Y., and Wang, R.F. (2007). Regulatory T cells and cancer. Curr. Opin. Immunol. *19*, 217–223.

Wang, Y., Kissenpfennig, A., Mingueneau, M., Richelme, S., Perrin, P., Chevrier, S., Genton, C., Lucas, B., DiSanto, J.P., Acha-Orbea, H., et al. (2008). Th2 lymphoproliferative disorder of LatY136F mutant mice unfolds independently of TCR-MHC engagement and is insensitive to the action of Foxp3+ regulatory T cells. J. Immunol. *180*, 1565–1575.

Woo, E.Y., Yeh, H., Chu, C.S., Schlienger, K., Carroll, R.G., Riley, J.L., Kaiser, L.R., and June, C.H. (2002). Cutting edge: Regulatory T cells from lung cancer patients directly inhibit autologous T cell proliferation. J. Immunol. *168*, 4272–4276.

Yu, P., Lee, Y., Liu, W., Krausz, T., Chong, A., Schreiber, H., and Fu, Y.X. (2005). Intratumor depletion of CD4+ cells unmasks tumor immunogenicity leading to the rejection of late-stage tumors. J. Exp. Med. *201*, 779–791.

Yu, G., Xu, X., Vu, M.D., Kilpatrick, E.D., and Li, X.C. (2006). NK cells promote transplant tolerance by killing donor antigen-presenting cells. J. Exp. Med. *203*, 1851–1858.

Zeelenberg, I.S., Ostrowski, M., Krumeich, S., Bobrie, A., Jancic, C., Boissonnas, A., Delcayre, A., Le Pecq, J.B., Combadière, B., Amigorena, S., and Théry, C. (2008). Targeting tumor antigens to secreted membrane vesicles in vivo induces efficient antitumor immune responses. Cancer Res. *68*, 1228–1235.

Zelenay, S., and Demengeot, J. (2006). Comment on "Cutting edge: Anti-CD25 monoclonal antibody injection results in the functional inactivation, not depletion, of CD4+CD25+ T regulatory cells". J. Immunol. *177*, 2036–2037, author reply 2037–2038.

Zhao, D.M., Thornton, A.M., DiPaolo, R.J., and Shevach, E.M. (2006). Activated CD4+CD25+ T cells selectively kill B lymphocytes. Blood *107*, 3925–3932.